Influence of raster and extrusion parameter over thermo-mechanical properties of ASA 3D printed samples

Andreea Isabela Danalache[1], *Mihai* Popa[1], *Bogdan* Pricop[1], *Constantin* Baciu[1], *Vasile* Ermolai[2*]

[1]Faculty of Materials Science, "Gheorghe Asachi" Technical University of Iași, Blvd. Dimitrie Mangeron 71A, 700050 Iasi, Romania
[2]Faculty of Machine Manufacturing and Industrial Management, "Gheorghe Asachi" Technical University of Iași, Blvd. Dimitrie Mangeron 59A, 700050 Iasi, Romania

Abstract. This study investigates the thermo-mechanical behavior of acrylonitrile styrene acrylate (ASA) specimens fabricated using Fused Filament Fabrication (FFF). The influence of raster width, raster angle, extrusion temperature, and flow rate were analyzed using Dynamic Mechanical Analysis (DMA). Results showed that raster angle and extrusion parameters significantly affect the storage modulus and glass transition temperature. Optimal stiffness was achieved at 45° raster orientation, 0.5 mm raster width, 240°C extrusion temperature, and a flow rate of 1.00. These findings highlight the importance of parameter selection for improving the performance of ASA components in thermally and mechanically demanding applications.

1 Introduction

Fused Filament Fabrication (FFF) is an extrusion-based additive manufacturing technology that uses thermoplastic materials to build parts layer wise [1–3]. A filament-shaped feedstock is fed into a heated zone, where it liquefies and is extruded through a nozzle. The material is then deposited sequentially in the form of filaments with defined shape, width, thickness, and orientation, creating the part's layers [2, 3].

FFF resulting parts consist of two main structural elements: external shell and internal structure. On the one hand, the outer geometry includes one or more solid shells, closed at the bottom and top by densely packed rasters, also known as solid fill. On the other hand, the internal structure, referred to as infill, if often printed at lower densities to reduce material usage and build time. The infill is defined mainly through pattern and density [4,5].

The final structure of an FFF part depends on a variety of process parameters, including layer height, infill pattern, infill density, raster orientation and slicing algorithm. Among these, raster orientation, described as the angle at which the material is deposited in each layer, plays a significant role in determining the mechanical and rheological behavior of the printed part [7, 8]. This parameter tries to explain how external loads are distributed across

* Corresponding author: vasile.ermolai@academic.tuiasi.ro

the deposited paths and between layers, thereby affecting tensile strength, stiffness, damping capacity, and the overall structural uniformity.

The layer-by-layer deposition inherently induces anisotropy within the part, particularly in the direction perpendicular to the build plane. This structural anisotropy can significantly influence performance under mechanical and thermal loading [9, 10].

In terms of rheological behavior, the properties of the molten polymer, such as viscosity, flow behavior, and cooling dynamics, critically influence the quality of interlayer adhesion. These factors directly affect the extent of molecular adhesion through mechanism such as adsorption, diffusion and coalescence [11].

This study investigates the effects of raster width, raster orientation, extrusion temperature, and material flow on the thermo-mechanical properties of samples fabricated from acrylonitrile styrene acrylate (ASA). The results indicate that process parameters substantially impact the material's thermo-mechanical behavior, primarily through their influence on inter-bead coalescence, void formation, and surface quality.

2 Materials and Methods

2.1 Design of experiment

The experimental design followed a Taguchi L9 orthogonal array, incorporating four factors at three levels of variation (see table 1) resulting in nine parameters configurations. These factors describe the characteristics of the solid fill periodical profile and its deposition.

Table 1. Design of L9 (3^4) orthogonal array.

Run order	RW (mm)	RA (°)	ET (°C)	FR	E' (MPa)
R1	0.4	0	240	0.95	704
R2	0.4	45	250	1	1149
R3	0.4	90	260	1.05	943
R4	0.5	0	250	1.05	1253
R5	0.5	45	260	0.95	1179
R6	0.5	90	240	1	1147
R7	0.6	0	260	1	751
R8	0.6	45	240	1.05	1319
R9	0.6	90	250	0.95	774
RW – Raster width;			*ET – Extrusion temperature;*		
RA – Raster angle;			*FR – Flow ratio.*		

Raster Width (RW) controls the extrusion width of the rasters or filaments. A lower value (i.e., 0.4 mm) results in narrower deposition paths, thereby reducing air gaps between adjacent filaments. Then, a higher value (i.e., 0.6 mm) increases the spacing and facilitates the formation of larger voids as illustrated in figure 1. The formation of these gaps may be further increased by under-extrusion during printing [12].

Raster Angle (RA) defines the orientation of the deposited lines within each layer (see figure. 1). This parameter influences filament packing efficiency and air gap formation due to variations in the print head trajectory and overlap. Prior studies have demonstrated that raster orientation significantly affects mechanical performance through its influence on anisotropy, internal porosity and load undertake [12].

Extrusion Temperature (ET) controls the processing temperature of the filament. Amorphous polymers such as ASA exhibit a broader melting range compared to semicrystalline materials or elastomers. At lower temperatures (e.g., 240°C), the polymer may not achieve full melt flow, leading to poor inter-bead bonding and the formation of voids. In contrast, higher extrusion temperatures (e.g., 260°C), while remaining below the

degradation threshold, reduce the melt's surface tension. This enhances filament wettability and interfacial adhesion, improving the mechanical properties of the resulting part.

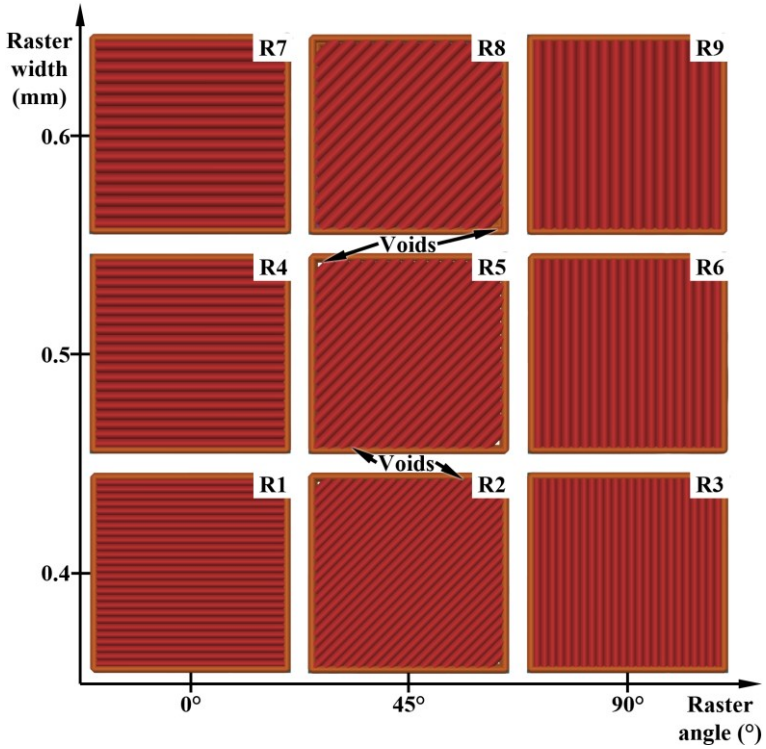

Fig. 1. The influence of RW and RA parameter over the periodic profile of the resulting parts.

Flow Rate (FR) is a slicer-specific parameter that defines the volumetric rate at which the material is extruded. It is expressed as a dimensionless value, where a default setting of 1 (or 100%) corresponds to the nominal extrusion rate of the printer. The actual maximum volumetric flow rate depends on both the extruder's capabilities and the rheological properties of the polymer. For the Bambu Lab A1 printer using ASA, the maximum flow rate reaches approximately 8 mm^3/s.

2.2 Experimental procedure

The experimental procedure aimed to investigate the mechanical and thermal behavior of ASA samples manufactured via FFF, with a specific focus on the influence of raster orientation (0°, 45°, and 90°). The study employed Dynamic Mechanical Analysis (DMA) to assess viscoelastic properties under dynamic loading.

To characterize the mechanical response of ASA under dynamic conditions, we prepared parallelepipedal specimens with dimensions of 1×4×50 mm. These samples were tested using a NETZSCH DMA 242 E Artemis instrument, equipped with a dual cantilever configuration. The primary objective of the DMA heating test was to determine the onset of the glass transition by monitoring the softening behavior of the storage modulus (E′) as a function of temperature. Specimens were heated from 23°C to 120°C at a constant rate of 3°C/min, while being dynamically loaded with a sinusoidal force at 1 Hz frequency and 100 µm amplitude.

In addition to the temperature sweep, we conducted stress sweep experiments at two characteristic temperatures: the temperature at which the storage modulus reached its

minimum, prior to the glass transition, and the temperature corresponding to the onset of the glass transition, identified as the peak in E′. For each condition, we incrementally increased the applied force from 1 to 6 N in 11 equal steps to investigate the material's stress-dependent mechanical response under dynamic loading.

2.3 Samples' printing

For this study, we used Apollo X, a colored ASA filament produced by the Dutch company Form Futura. This engineering-grade thermoplastic offers resistance to ultraviolet radiation and demonstrates good mechanical performance. Prior to printing, the filament spool underwent dehydration in a Sunlu S4 FilaDryer at 70°C for 8 hours. During printing, the filament was stored in a sealed dry box containing silica desiccant to maintain a relative humidity of 14%.

We performed the slicing and process parametrization using Orca Slicer 2.3.0, an open-source slicing software. The experimental setup followed the variable configurations presented in Table 1, with the remaining process parameters detailed in table 2. Notably, the raster orientation remained constant throughout the part height and was not alternated by 90° between consecutive layers. Each sample maintained the same raster angle from the base to the top layer, in accordance with the orientation specified in Table 1.

Table 2. Main process parameters used for printing the samples.

No.	Parameter	Value
1	Nozzle diameter (mm)	0.4
2	Layer thickness (mm)	0.2
3	Number of walls	1
4	Top/bottom layers	3
6	Printing speed (mm/s)	50
6	First layer printing speed (mm/s)	20
7	Bed temperature (°C)	100
8	Maximum fan speed (%)	5
9	Retraction distance (mm)	0.8
10	Retraction speed (mm/s)	30
11	Z seam position	Sharpest corner
12	Brim width (mm)	5
13	Enclosure	Yes

All samples were fabricated in batches of five using a Bambu Lab A1 printer housed in a Top Cube enclosure. For each of the nine experimental configurations, the enclosure was preheated to 40°C prior to printing. Relative humidity during fabrication was maintained between 37% and 42%.

As illustrated in figure 2, the top surface topography of the printed specimens varied significantly depending on the experimental Taguchi L9 matrix configuration. Across all combinations of raster width and orientation, the FR exerted a noticeable influence on the periodic profile of the raster lines. For samples printed with an FR of 0.95 (R1, R5, and R9), visible voids appeared between adjacent rasters due to insufficient material flow. In contrast, samples printed with an FR of 1.05 (R3, R4, and R8) exhibited a pronounced deterioration in surface quality, likely caused by material overflow. This phenomenon was also partially observed in some of the samples printed at a nominal FR of 1.00 (R2, R6, and R7).

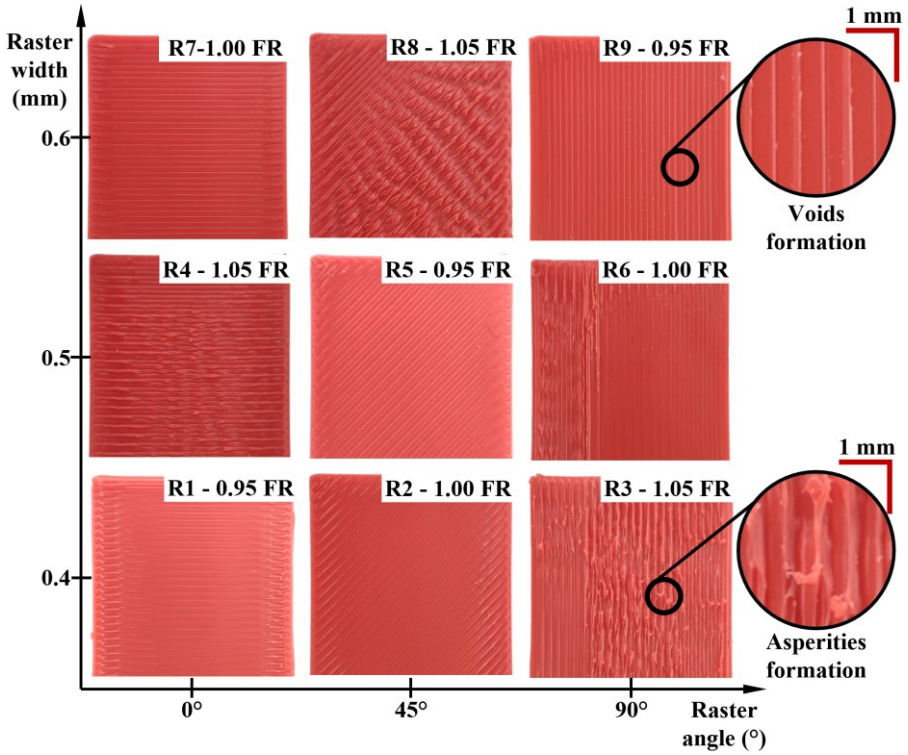

Fig. 2. Top view of the Taguchi L9 parametrization resulting samples.

Under standard FFF conditions, alternating raster angles between layers (typically by 90°) enhance mechanical performance by promoting interlayer fusion and achieving a more uniform melt distribution, by filling intralayer voids. In this study case, the use of a fixed raster orientation throughout the height of the sample may have reduced inter-raster void filling and facilitated melt displacement from the extrusion path, thereby contributing to the formation of surface asperities, as shown in figure. 2.

3 Results and discussion

The experimental plan employed on the DMA samples comprised a series of variables, including RW, RA, ET, and FR. In light of the variables above, nine distinct specimen types were obtained, and their printing settings are presented in Table 1.

To determine the influence of the raster deposition angle on the variation of storage modulus E' registered on heating, samples R1, R2, and R3 were plotted on the same graph presented in figure 3. As shown, increasing the raster angle from 0° (R1) to 45° (R2) resulted in a reduction of approximately 9°C in the glass transition onset temperature (Tg). Simultaneously, the storage modulus increased by 63%, from 704 MPa to 1150 MPa, indicating a notable enhancement in elastic stiffness.

A further increase in the deposition angle to 90° resulted in a decrease of only 3°C in the Tg starting temperature and a slight increase in the storage modulus, from 704 to 943 MPa. These results indicate that increasing the raster angle contributes to a stiffer material response while slightly reducing the glass transition temperature, likely due to improved alignment of load-bearing paths along the principal stress directions.

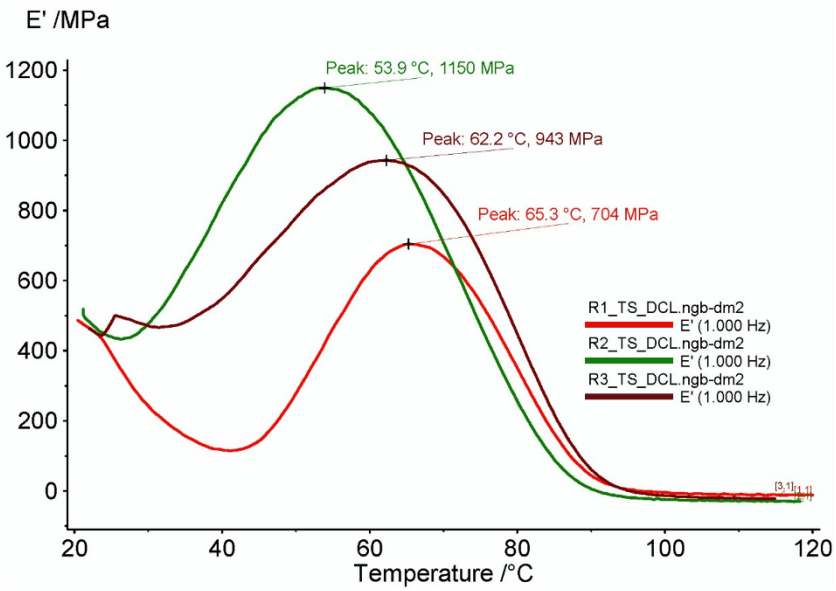

Fig. 3. The influence of the raster angle on the variation of storage modulus E' on heating.

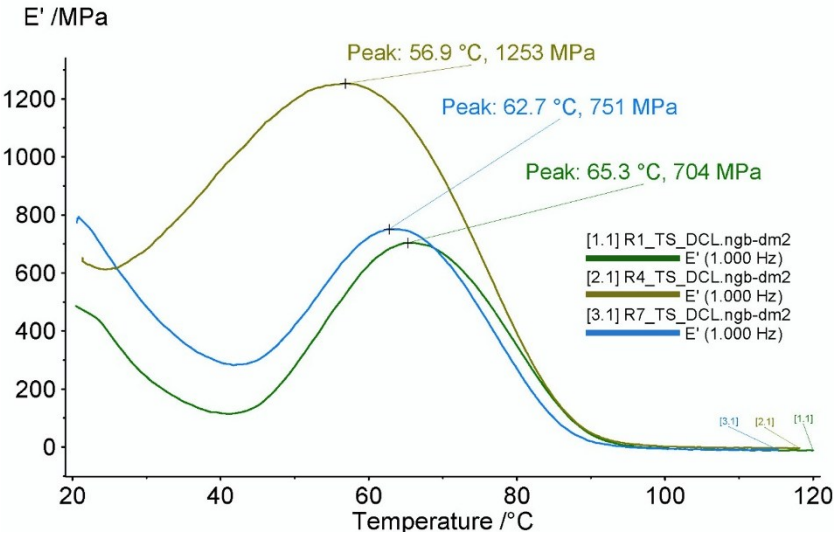

Fig. 4. The influence of the raster width on the variation of storage modulus E' on heating.

The graph shown in figure 4 illustrates the influence of raster width on the variation of the storage modulus (E′), comparing samples printed with widths of 0.4 mm, 0.5 mm, and 0.6 mm. Between the 0.4 mm and 0.6 mm configurations, only minor differences were observed, approximately 2°C in the glass transition onset temperature and 47 MPa in E′. However, the intermediate raster width of 0.5 mm led to a notable increase of 79% in the storage modulus, while the glass transition temperature varied by just 8°C, indicating a balance between stiffness and thermal stability.

The effect of extrusion temperature on the elastic response is shown in figure 5. Samples printed at 240°C demonstrated the highest stiffness. Increasing the extrusion temperature beyond this point resulted in a significant decrease in E′, with samples becoming up to 90% less stiff, highlighting the detrimental effect of excessive heat on interlayer adhesion.

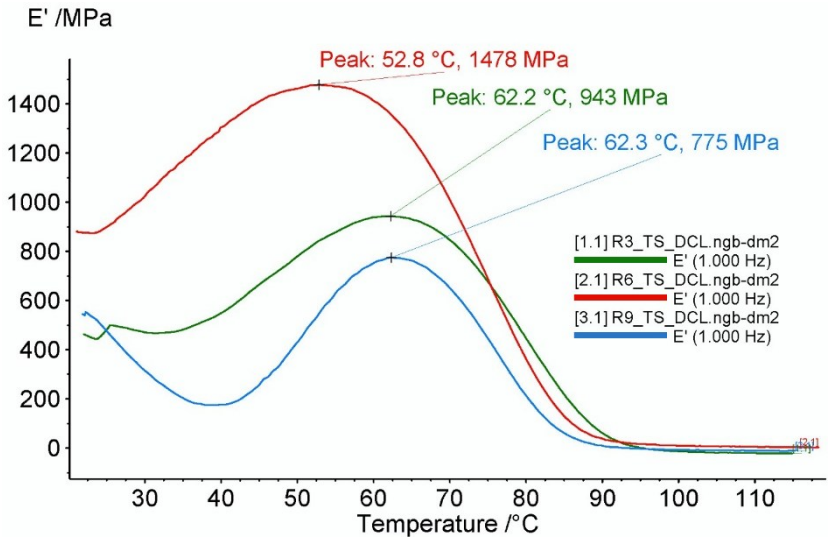

Fig. 5. The influence of the extrusion temperature on the variation of storage modulus E' on heating.

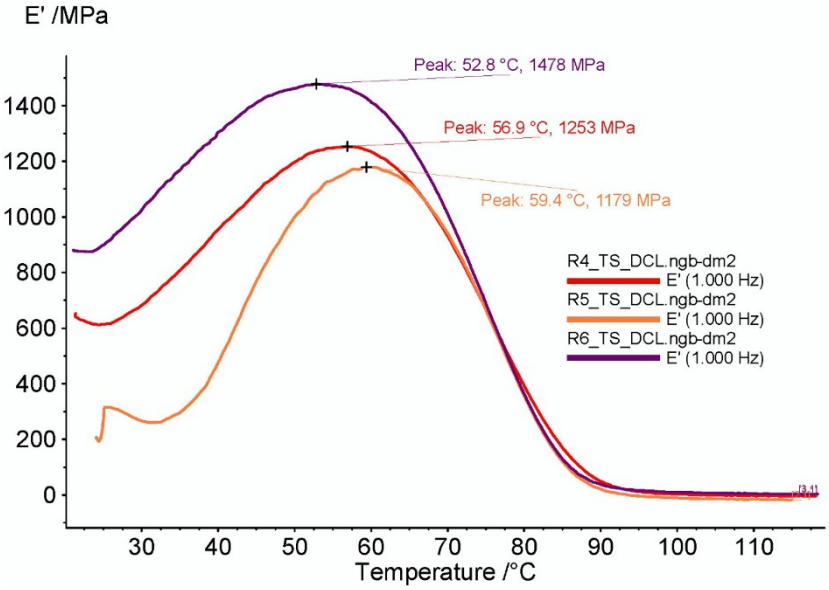

Fig. 6. The influence of the flow ratio on the variation of storage modulus E' on heating.

The influence of FR on the storage modulus is highlighted in figure 6. Among the tested values (0.95, 1.00, and 1.05), the nominal flow rate of 1.00 yielded the highest E′, reaching approximately 1480 MPa. In contrast, reducing the flow rate to 0.95 resulted in a lower stiffness of 1179 MPa, likely due to insufficient material deposition and increased voids sizes between rasters.

The stress sweep behavior of samples R1-R3 is shown in figure 7. As outlined in the Materials and Methods section, each sweep was conducted at two distinct temperatures. The dotted lines in the figure correspond to the high-temperature sweeps. Among the three specimens, sample R3, tested at 32°C, exhibited the highest strain response. Although sample R2 was tested at a lower temperature (i.e., 26°C), it displayed lower strain values than R3. When tested at elevated temperatures (≈60°C), the strain responses across all three samples

became more similar, indicating a convergence in viscoelastic behavior near the glass transition temperature. Notably, sample R1 demonstrated the smallest difference between low and high-temperature sweeps, indicating greater stability across temperature ranges.

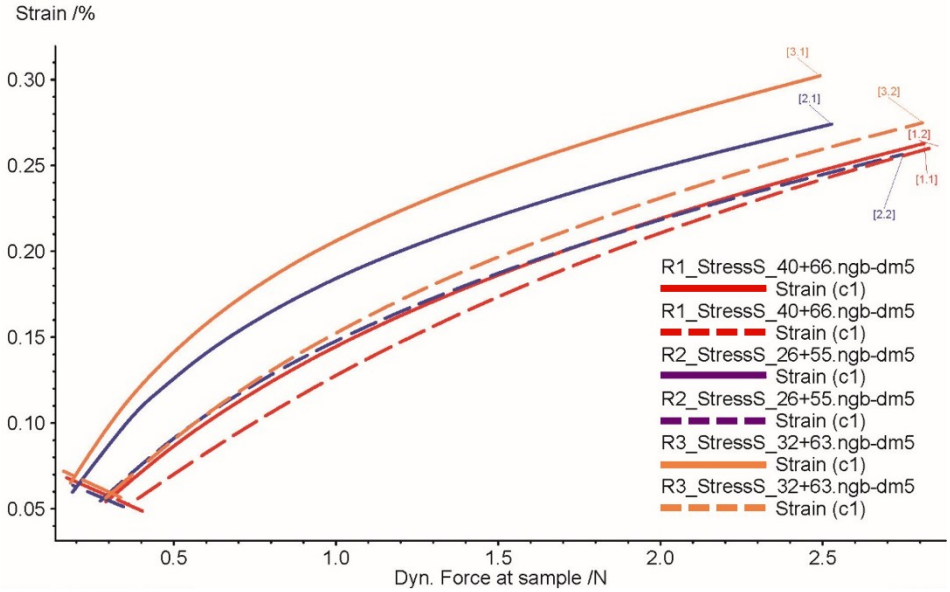

Fig. 7. Stress sweeps were recorded at two different temperatures on R1 to R3 samples.

The graphs presented in figure 8. present the results for samples R4 to R6. Similar to the previous set, distinct differences between the low and high-temperature sweeps were observed. However, the response at the higher temperature appeared more uniformly distributed across these three samples, showing a consistent material softening behavior under increased thermal loading.

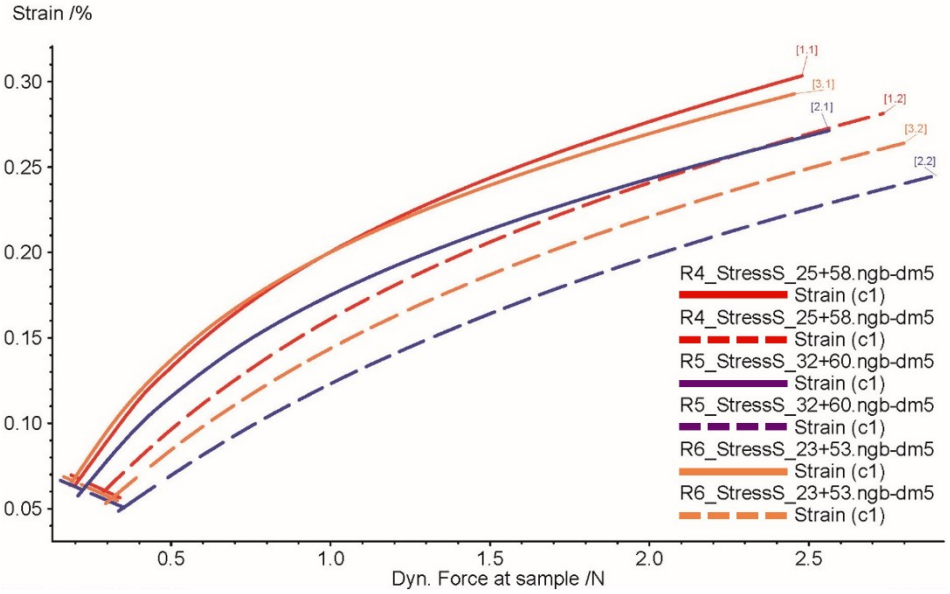

Fig. 8. Stress sweeps were recorded at two different temperatures on R4 to R6 samples.

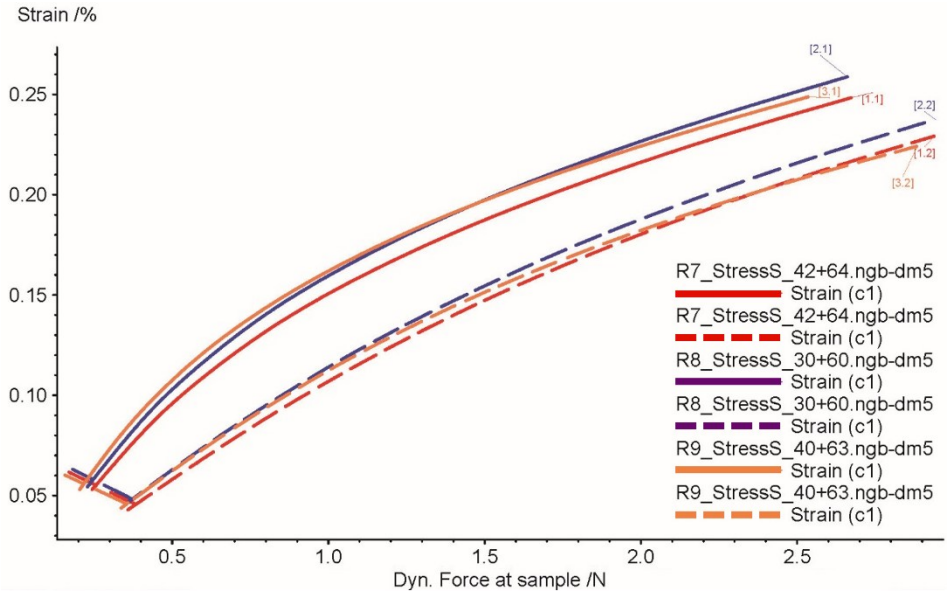

Fig. 9. Stress sweeps were recorded at two different temperatures on R7 to R9 samples.

The final set, samples R7 to R9, is displayed in figure 9. In contrast to the previous groups, all three samples exhibited nearly identical behavior at both testing temperatures, despite the sweeps being conducted at different values. This uniformity may indicate that these process parameters resulted in material structures less sensitive to thermal variation during dynamic loading.

4 Conclusions

This study evaluated the thermo-mechanical behavior of ASA samples fabricated via Fused Filament Fabrication. The influence of raster width, raster angle, extrusion temperature, and flow rate were assessed through DMA analyses to understand their effect on storage modulus, stress response.

Results show that increasing the raster angle significantly improves stiffness, with a maximum storage modulus increase of 63% observed at 45°, though accompanied by a slight decrease in glass transition temperature. Raster width also had a notable impact, with the 0.5 mm configuration yielding the highest E′, indicating optimal filament adhesion.

Extrusion temperature and flow rate emerged as critical parameters. A temperature of 240°C ensured the best mechanical performance, while higher values led to softening. Similarly, a nominal flow rate (i.e., 1.00) resulted in maximum stiffness, whereas under or over-extrusion affected structural integrity and surface quality.

References

1. Yadav, P. Rohru, A. Babbar et al., Fused filament fabrication: a state-of-the-art review of the technology, materials, properties and defects, Int. J. Interact. Des. Manuf. 17, 2867–2889 (2023)
2. Gibson, D. Rosen, B. Stucker, M. Khorasani, Material extrusion, in Additive Manufacturing Technologies, Springer Nature, Switzerland, 171–201 (2021) ISBN 978-3-030-56127-7

3. S.W.T. Tientcheu, J.M. Djouda, M.A. Bouaziz et al., A review on fused deposition modeling materials with analysis of key process parameters influence on mechanical properties, Int. J. Adv. Manuf. Technol. 130, 2119–2158 (2024)
4. S. Terekhina, I. Skornyakov, T. Tarasova, S. Egorov, Effects of the infill density on the mechanical properties of nylon specimens made by filament fused fabrication, Technologies 7(3), 57 (2019)
5. Yankin, Y. Alipov, A. Temirgali et al., Optimization of printing parameters to enhance tensile properties of ABS and nylon produced by fused filament fabrication, Polymers 15(14), 3043 (2023)
6. R.C. Stavarache, V. Ermolai, M.I. Ripanu, L. Andruşcă, M. Mareş, O. Dodun, Infill pattern optimization of fused filament fabrication samples for enhanced mechanical properties, Sci. Bull. Ser. C Fascicle Mech.
7. M. Alagheband, Q. Zhang, S. Jung, Investigating the influence of infill patterns and mesh modifiers on fatigue properties of 3D printed polymers, Int. J. Fatigue 187, 108463 (2024)
8. H.K. Dave, B.H. Patel, S.R. Rajpurohit, A.R. Prajapati, D. Nedelcu, Effect of multi-infill patterns on tensile behavior of FDM printed parts, J. Braz. Soc. Mech. Sci. Eng. 43(1), 23 (2021)
9. J. Ghorbani, P. Koirala, Y.L. Shen, M. Tehrani, Eliminating voids and reducing mechanical anisotropy in fused filament fabrication parts by adjusting the filament extrusion rate, J. Manuf. Process. 80, 651–658 (2022)
10. Y. Tao, F. Kong, Z. Li et al., A review on voids of 3D printed parts by fused filament fabrication, J. Mater. Res. Technol. 15, 4860–4879 (2021)
11. D. Acierno, A. Patti, Fused deposition modelling (FDM) of thermoplastic-based filaments: process and rheological properties-an overview, Materials 16(24), 7664 (2023)
12. V. Ermolai, A. Sover, G. Nagîț, M.A. Boca, A.I. Irimia, Influence of fused filament fabrication raster parameters over the top surface topography, Acta Tech. Napoc. Ser. Appl. Math. Mech. Eng. 66(5) (2023)